Signal Processing 93 (2013) 1864–1870

Contents lists available at SciVerse ScienceDirect

Signal Processing

journal homepage: www.elsevier.com/locate/sigpro

Characterization of bio-dynamic speckles through classical and fuzzy mathematical morphology tools

Eduardo Blotta [a,*], Agustina Bouchet [a,b], Marcel Brun [a], Virginia Ballarin [a]

[a] Grupo de Procesamiento Digital de Imágenes, Facultad de Ingeniería, U.N.M.D.P. Mar del Plata, Argentina
[b] Consejo Nacional de Investigaciones Científicas y Técnicas (CONICET), Argentina

ARTICLE INFO

Article history:
Received 2 May 2012
Received in revised form
26 October 2012
Accepted 4 January 2013
Available online 1 February 2013

Keywords:
Dynamic speckle
Mathematical morphology
Fuzzy mathematical morphology
Morphological granulometric function

ABSTRACT

In this paper we characterize dynamic speckle signals, obtaining selective information through the differentiation of morphological patterns of the temporal history of each pixel, using the morphological granulometric function. This method is applied to the analysis of images of apples and corn seeds. Studies on the first ones were focused on the activity on their surface, related to healthy and damaged areas, while for seeds on the viability of the embryo and endosperm. Subsequently, the analysis was repeated using fuzzy mathematical morphology techniques, comparing the results obtained by both methods.

1. Introduction

When a surface that has physical or biological activity is illuminated by coherent light, such as a laser, the scattered light displays a granular structure, i.e. presenting randomly distributed light and dark spots, which change over time, giving a visual effect of "water boiling". This effect is known as "dynamic" speckle or "bio-speckle". This phenomenon has been studied in various types of biological samples, such as fruits [15] and seeds [7]. Various methods and techniques have been developed for measuring the activity of a speckle pattern [8,1], but, in most cases, the results consist of a single image, with no analysis of the temporal information. Subsequently, selective filtering techniques were used for studying the bio-speckle signals through spectral decomposition [16,11]. Going in the same direction, we introduced recently a new method for bio-speckle analysis based on the morphological spectrum obtained by morphological granulometry [4,3,5].

This technique is based on the theory of mathematical morphology (MM) [14,17], which is a powerful set of tools for digital image processing. These techniques allow enhancement of diffuse areas, object segmentation, edge detection and structures analysis via the use of operators or filters. This discipline is based on sets algebra and can be also be used as a tool for signals analysis. The techniques, initially developed for binary images, were also extended to the field of gray level images. Another approach to extend binary operators to gray level images, the fuzzy mathematical morphology (FMM), is based on fuzzy sets theory. Often, the fuzzy operators result more robust than classical morphological operators [6].

When illuminated by a laser light, fruits show an speckle activity that can be related to the degree of maturity, turgor pressure, damage, age and mechanical properties. For this reason, it is interesting to develop numerical methods which allow to extract useful information of the speckle image sequences.

On the other hand, the study of the feasibility of germination is an important topic in production and marketing seeds.

* Corresponding author. Tel.: +54 223 474 5994.
E-mail address: eblotta@fi.mdp.edu.ar (E. Blotta).

0165-1684/$ - see front matter © 2013 Elsevier B.V. All rights reserved.
http://dx.doi.org/10.1016/j.sigpro.2013.01.001

They have been developed many tests to determine strength and viability of seed germination. Other studies about the reliability of the tests and equivalence between them also exist [12]. In this context, the evaluation of laser interferometry techniques as tools for seeds analysis is worthy to take into account.

In this paper, we apply MM and FMM filters to biological samples of red delicious apples, as a tool for the diagnostic of early damage of the surface of the fruit, and to corn seeds, to study its performance in the germination process.

2. Methods

2.1. Dynamic speckle

When a surface, that has a certain physical or biological activity, is illuminated by a high coherence light beam, the scattered light by the surface has a granular structure composed of small bright and dark areas, randomly distributed, which change over time, producing an visual effect as a boiling liquid.

Fig. 1 shows a typical image. This effect, known as "dynamic speckle", is a result of coherent light scattering by objects that exhibit some level of activity. These type of images present variations in the local intensity corresponding to the level of biological activity in the area under observation. Fig. 2 shows the temporal evolution of the intensity of a sample pixel, or gray levels, in a typical sequence of dynamic speckle images. Due to the stochastic nature of the signal, it would be impossible with the naked eye recognize the correspondence of this with any particular area of a biological sample.

The dynamics of the speckle effect is usually quite complex due to multiple physical mechanisms involved [18], but the activity evaluation can help to recognize the complex processes occur in a biological sample.

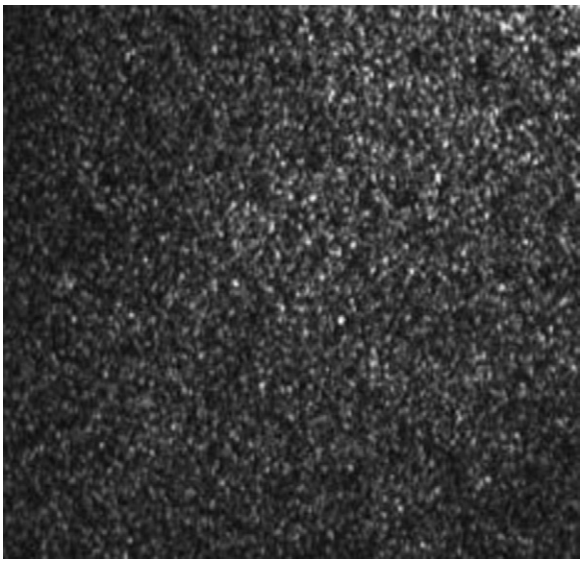

Fig. 1. Typical speckle pattern.

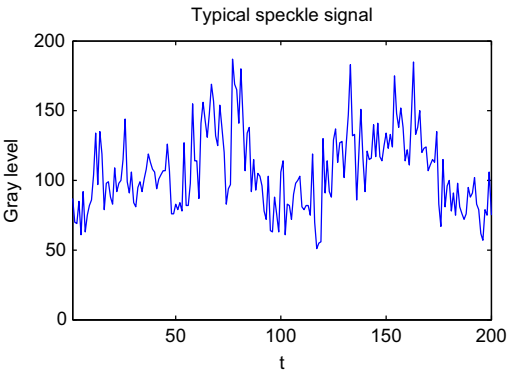

Fig. 2. Typical temporal evolution of a bio-speckle.

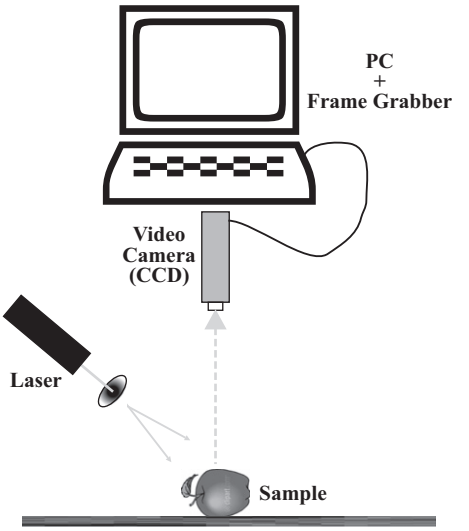

Fig. 3. Experimental speckle bank.

2.2. Experiments

The test bank used to obtain the images is shown in Fig. 3. We used a low-power He–Ne laser (5 mW, $\lambda = 633$ nm) to illuminate the samples, using a divergent beam expanded to encompass a wide region. Subjective speckle images were formed by a objective (usually $f=50$ mm, $f/\#=16$). Thus, measurement of average speckle grains covered several pixels. For the experiment with apples, an inert reference object was added in the images. Successive images were stored on a PC by a CCD camera connected to a acquisition board. Low lighting levels were used so that the effect of irradiation on the sample was negligible. The laser illumination was adjusted to keep constant the average intensity in the image throughout the test.

To study variations of the speckle phenomenon in the surface of the fruit, a controlled hit was applied to the healthy apples. That hit was caused by a falling steel ball ($dm=21.9$ mm, $weight=33.6$ g) from a height of 20 cm of fruit surface. The damage in the sample could not be appreciated by simple visual inspection. Images were

acquired in 300×300 pixels, digitized into 256 gray levels, each 0.5 s approximately. Sequences took 500 pictures before, and immediately after the coup.

Described image sequences were stored in 3D arrays $(300\times300\times256)$ where the third variable is the time. Thus, the temporal evolution of each pixel can be analyzed to detect changes in biological activity due to changes in the surface of the fruit.

In the case of seeds, experiments cited by the original paper [7] were held to explore how moisture affects speckle activity. This work, however, was focused on the qualitative aspects of the samples and the different morphologies in order to segment the interest areas of the seed, for analysis. We used specimens of corn seeds, previously wetted, cutted in half and we took sequences of 100 images of 256×480 pixels, using the bank previously described, with the same configuration.

2.3. Mathematical morphology

The basic image operators of the mathematical morphology (MM) are the *dilation* and the *erosion*. Many other operators of the MM are built combining these two operators.

We will describe in this section the morphological operators used for the analysis of the unidimensional bio-speckle signals, defined by $f: D\subset\mathbb{Z}\rightarrow\{0,1,2,\ldots,255\}$, where $\mathbb{Z}$ is the set of integer numbers.

The *dilation* of the signal f by the signal b, called also *structuring element* (SE) is defined by [17]

$$\delta(f,b)(x)=\sup_{y\in D_b}\{f(x-y)+b(y)\} \tag{1}$$

where $x\in D_f$, and D_f and D_b are the support of f and b, respectively.

The same way we define the *erosion* of the signal f by the signal b, by [17]

$$\varepsilon(f,b)(x)=\inf_{y\in D_b}\{f(x-y)-b(y)\} \tag{2}$$

Based on these two operators of dilation and erosion, the *opening* is defined as the combination of a erosion followed by a dilation:

$$\gamma(f,b)=\delta(\varepsilon(f,b),b) \tag{3}$$

Both, the operator and the SE chosen, will determine the characteristics of the resulting processed signal.

Fig. 4 shows the effect on the signal obtained by the application of a morphological opening to a bio-speckle signal, with a linear SE of length 2.

If we consider $\Omega(f_0)$ the area under the original signal, and $\Omega(f_n)$ the area under the signal f_n, obtained by applying an opening to f_0 with a lineal SE of length n, we can define the *granulometric size distribution* $\phi(n)$, or GSD [9], by

$$\phi(n)=1-\frac{\Omega(f_n)}{\Omega(f_0)},\quad n=0,\ldots,N \tag{4}$$

$\phi(n)$ is a non-decreasing function, similar to statistical cumulative distribution, but without reaching the value one, which is fixed later by a normalization factor. It represents the variation of the area under the signal as it is probed by increasing shapes (the SE), which can be compared to a selective filtering of the shape of the signal, since the signal is smoothed with more strength in each iteration. The operation ends for a value $n=N$, which depends on the shape of the signal, when there is no variation between two consecutive openings.

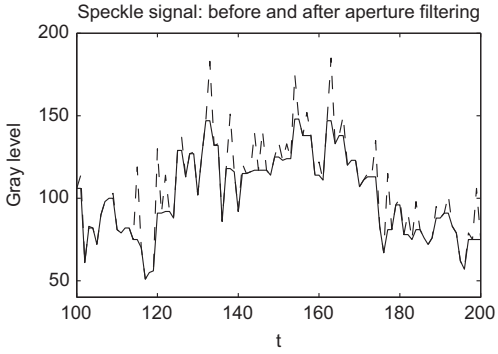

Fig. 4. Morphological opening applied on a bio-speckle signal.

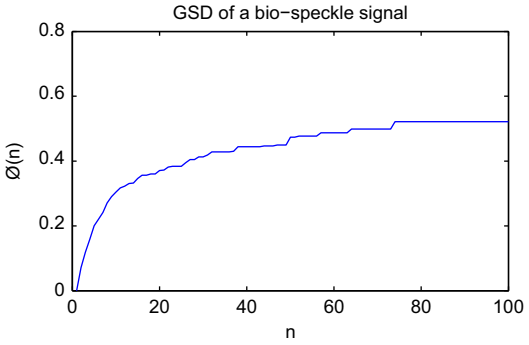

Fig. 5. Example of the granulometric size distribution for a bio-speckle signal.

Fig. 5 shows an example of *GSD* calculated for the signal of Fig. 4.

2.4. Fuzzy mathematical morphology

The fuzzy mathematical morphology (FMM) provides a way to extend mathematical morphology's binary operators to gray level images, extending the set operations to fuzzy set ones, based on the theory of fuzzy sets. Fuzzy sets are defined by their "membership" function, with values in the interval [0,1] [10].

For the unidimensional case, gray level signals with range between 0 and 255 can be "fuzzified" to fit in the [0,1] range, via the function $g:\{0,1,2\ldots,255\}\rightarrow[0,1]$

$$g(x)=\frac{x}{255} \tag{5}$$

It is important to note that this does not mean that the signal represents a fuzzy membership function for some object, this is just a way to model the gray level signal to be able to apply morphological operators defined via fuzzy set operations. Signals can be defuzzified by applying

$h : [0,1] \rightarrow \{0,1,2 \ldots ,255\}$ defined by

$$h(x) = [255 \cdot x] \tag{6}$$

where $[.] : \mathbb{R} \rightarrow \mathbb{Z}$ represents the function

$$[a] = \sup\{k \in \mathbb{Z} / k \leq a\} \tag{7}$$

In this framework, the fuzzy morphological dilation of a signal f by a SE b is defined by [2,6]

$$\delta^F(f,b)(x) = \sup_{y \in D_b} \{T(f(y), b(y-x))\} \tag{8}$$

where $T[a,b]$ is a T-norm [10].

The fuzzy morphological erosion of the signal f by the SE b is defined by [2,6]

$$\varepsilon^F(f,b)(x) = \inf_{y \in D_b} \{S(f(y), c(b(y-x)))\} \tag{9}$$

where $S[a,b]$ is a T-conorm and $c(a) = 1-a$ is the fuzzy complement [13].

Fuzzy opening is defined in the same way as in the MM. The fuzzy opening $\gamma_b^F(f)$ of the signal f by the signal b is defined by

$$\gamma(f,b)_b^F = \delta^F(\varepsilon^F(f,b),b) \tag{10}$$

In this work we used a set of T-norms and T-conorms, which provide different fuzzy morphology operators (Tables 1 and 2), choosing to show only results for the best ones: *standard* and *Dubois & Prade*.

Table 1
T-norms.

	T-norm
Standard	$T(a,b) = \min(a,b)$
Algebraic	$T(a,b) = ab$
Bounded	$T(a,b) = \max(0, a+b-1)$
Drastic	$T(a,b) = \begin{cases} a & \text{for } b=1 \\ b & \text{for } a=1 \\ 0 & \text{cc} \end{cases}$
Dubois & Prade[a]	$T(a,b) = 1 - \frac{(1-a)(1-b)}{\max(1-a, 1-b, \gamma)}$
Hamacher[b]	$T(a,b) = \frac{ab}{\gamma + (1-\gamma)(a+b-ab)}$

[a] γ belong to the interval (0,1).
[b] γ must be positive.

Table 2
T-conorms.

	T-conorm
Standard	$S(a,b) = \max(a,b)$
Algebraic	$S(a,b) = a+b-ab$
Bounded	$S(a,b) = \min(1, a+b)$
Drastic	$S(a,b) = \begin{cases} a & \text{for } b=0 \\ b & \text{for } a=0 \\ 1 & \text{cc} \end{cases}$
Dubois & Prade[a]	$S(a,b) = 1 - \frac{(1-a)(1-b)}{\max(1-a, 1-b, \gamma)}$
Hamacher[b]	$S(a,b) = \frac{a+b+(\gamma-2)ab}{1+(\gamma-1)ab}$

[a] γ belong to the interval (0,1).
[a] γ must be positive.

Fuzzy granulometry is obtained applying the fuzzy opening. $\Omega(f_0)$ is the area under the original signal, and $\Omega(f_n^F)$ is the area under the signal f_n^F, which is obtained by opening of f_0 using a SE of length n. The *fuzzy granulometric size distribution* $\phi^F(n)$, or FGSD, is defined by

$$\phi^F(n) = 1 - \frac{\Omega(f_n^F)}{\Omega(f_0)}, \quad n = 0, \ldots, N \tag{11}$$

$\phi^F(n)$ is a non-decreasing function, similarly to $\phi(n)$.

3. Results

Fig. 6, shows the results of the GSD for on the speckle signal for apples, using three different SEs, (a)–(c), and the results of the FGSD for the same signal and SEs, (d)–(f), using the *Dubois & Prade* norms, and finally the results of the FGSD using the *standard* norm, (g)–(i).

In the images displayed in Fig. 6, showing the results of the analysis of bio-speckle for apples, the lower left corner shows a dark region, with no activity, associated to a steel plate placed in the area for reference. On the right side of the images we can see a brighter round area, displaying higher activity, corresponding to the place where the apple was hit. The rest of the apple, free of mechanical damages, shows intermediate values of activity.

Fig. 6(a), (d) and (g) shows a light filtering, removing only the most prominent peaks of the signals, due to the small length of the SE, of 2 pixels. Fig. 6(b), (e) and (h) shows a stronger filtering, with SE of length 10, which removed larger peaks of the signal. Finally, Fig. 6(c), (f) and (i) shows a strong filtering of most of the peaks of the signals, with an SE of length 30. Larger SEs were tried, with no further results, which may suggest a spectral density, compatible with previous works based on filter banks [16].

Fig. 6(b) and (c), processed with MM, shows clearly the place where the apple was hit, while the images processed with FMM do not show higher sensibility to the hit, except for Fig. 6(d) and (g), but made visible some dark regions, no visible in the images of the MM, with some specific activity not associated to the mechanical damage, worthy to study in subsequent research.

To quantify the segmentation performance of the different filtering methods, based on our knowledge about the three interest regions, we chose the best classified image to build a synthetic image, as a gold standard, with the mean values of the three regions, segmented manually, which was compared to the apple images (a)–(g) obtained by the morphological analysis, computing their mean square error (MSE). Lower values mean better segmentation performance. Table 3 shows the MSE for the different techniques and SE lengths. Results show that classic filtering with a SE of length 10 perform the best segmentation.

Same morphological techniques were applied on the corn seed, previously hydrated to force it to start the germination process, and cut in two parts. Fig. 7 displays a characterization of such seed. In this kind of seed the cotyledon absorbs the food reserves from the endosperm. The coleoptile is the protective sheath covering the

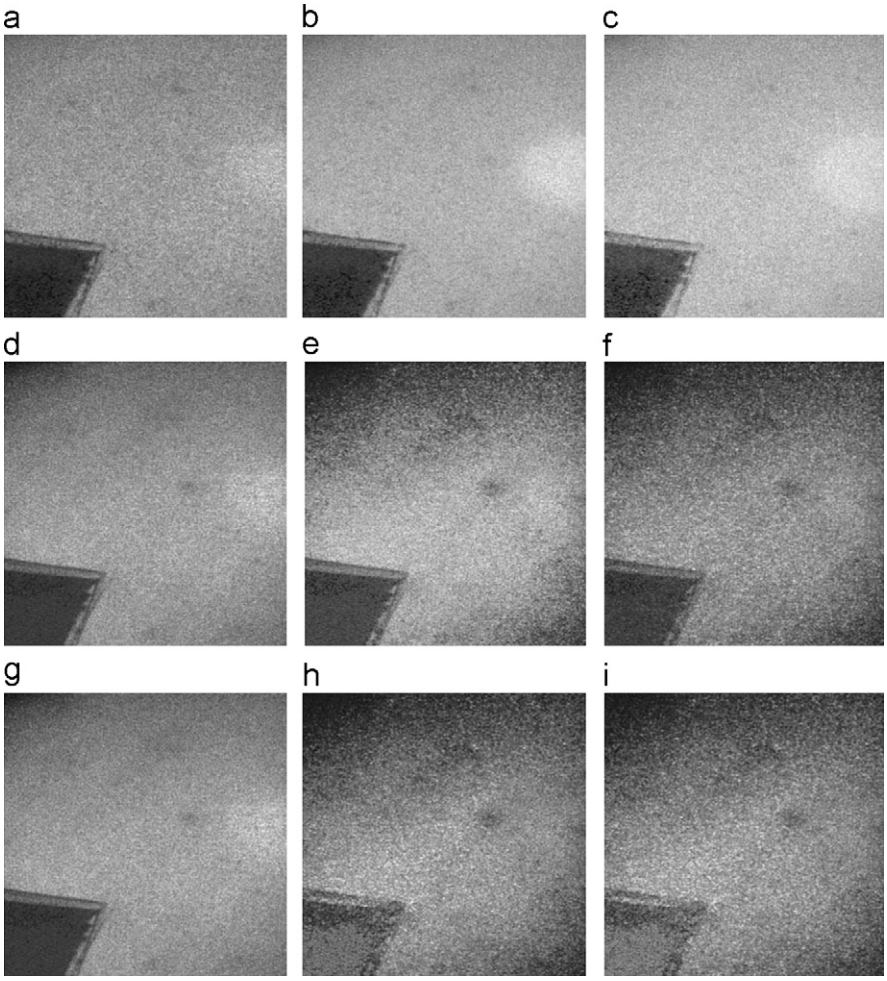

Fig. 6. Apple images after morphological filtering (SE lengths: 2, 10 and 30): (a)–(c) $\phi(2)$, $\phi(10)$ and $\phi(30)$, respectively. (d)–(f) $\phi^F(2)$, $\phi^F(10)$ and $\phi^F(30)$, using *Dubois & Prade* norms. (g)–(i) $\phi^F(2)$, $\phi^F(10)$ and $\phi^F(30)$, using *standard* norms.

Table 3
Mean of square quadratic errors between gold standard apple image and filtered speckle image. Lower values mean better segmentation performance.

Granulometry	$SE=2$	$SE=10$	$SE=30$
Classic	0.5356	0.3978	0.7796
Dubois & Prade	0.7691	2.0664	2.2075
Standard	0.7691	2.9491	2.9472

hypocotil, and it is the first structure to raises from the soil during germination.

Fig. 8, shows the results of the GSD for on the speckle signal for corn, using three different SEs, (a)–(c), and the results of the FGSD for the same signal and SEs, (d)–(f), using the *Dubois* & *Prade* norms, and finally the results of the FGSD using the *standard* norm, (g)–(i).

Fig. 8 shows the results for corn. In images (a)–(c), obtained by using MM, we can see a major contrast between the different regions, while images (d)–(i), obtained by FMM (*Dubouis* & *Prade* and *standard* norms), show uniform gray levels in the embryo region.

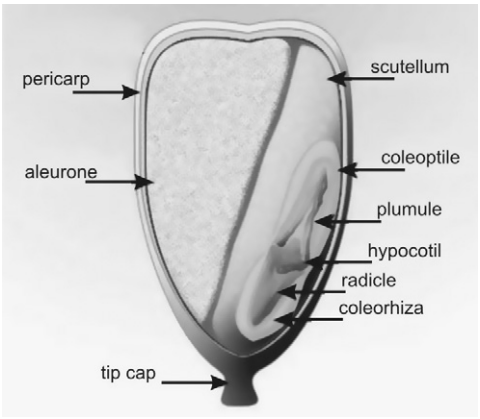

Fig. 7. Constitutive parts of a corn seed.

Table 4 shows the MSE computed for corn seed, contrasted to a hand-drawn image, with optimal segmented corn regions of embryo and endosperm. Lower values mean better segmentation performance.

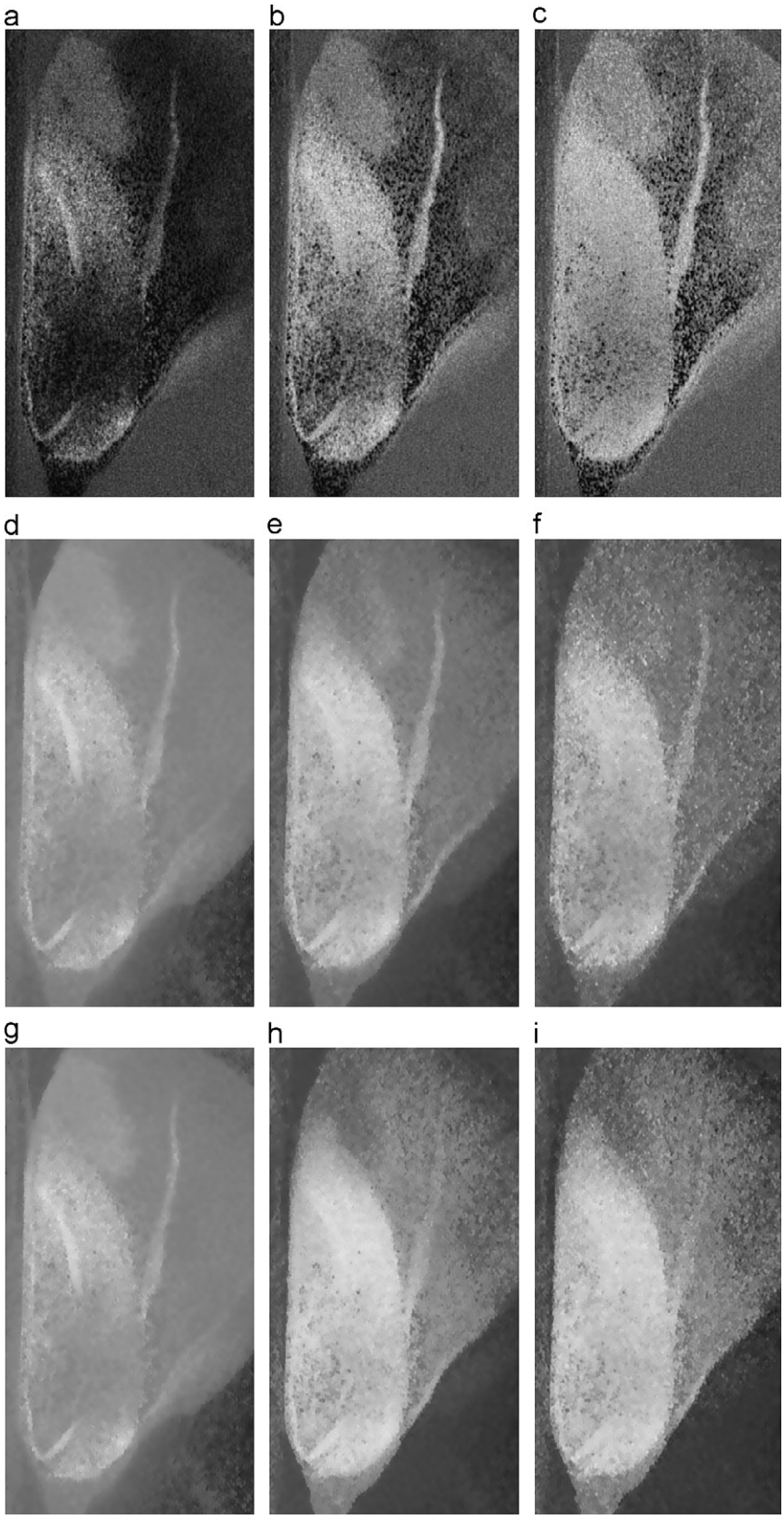

Fig. 8. Corn seed images after morphological filtering (SE lengths: 2, 10 and 30): (a)–(c) $\phi(2)$, $\phi(10)$ and $\phi(30)$, respectively. (d)–(f) $\phi^F(2)$, $\phi^F(10)$ and $\phi^F(30)$, using *Dubois & Prade* norms. (g)–(i) $\phi^F(2)$, $\phi^F(10)$ and $\phi^F(30)$, using *standard* norms.

Table 4
Mean of square quadratic errors between gold standard corn seed image and filtered speckle image. Lower values mean better segmentation performance.

Granulometry	$SE=2$	$SE=10$	$SE=30$
Classic	6.1600	2.0376	1.4473
Dubois & Prade	2.3611	2.1571	2.0519
Standard	2.3611	2.7069	2.8384

In most of the images, mainly for (a)–(c), we can detect constitutive elements of the embryo, brighter that the rest of the image, with different degrees of detail. The other important region, regarding seed viability, the endosperm, shows darker level. We can also see that FMM tends to uniform the gray levels for embryo, differentiating correctly embryo from endosperm. In order to improve the analysis of the results, further analysis by biologist will be required.

4. Conclusions

Application of dynamic speckle techniques for determining properties in various biological samples, such as fruits and seeds, has been considered in several studies using different approaches and getting different results. In this paper we showed the advantages of the use of morphological tools in the analysis of bio-speckle signals and we also made a comparison with latest widespread tools as is the fuzzy mathematical morphology.

Good results were obtained by calculating the granulometric size distribution of the speckle sequences, with a satisfactory level of detail. The granulometry is a "sieving" method with a reduced computational cost, in part because of its use of integer arithmetic.

On the other hand, the computational cost of using granulometry based on fuzzy mathematics does not increase significantly over classical granulometry. As for the feasibility to become a viable technique for the analysis of dynamic speckle signals, deeper studies of the biological field must be done by specialists to draw major conclusions, but a priori, it can be observed that may be effective as complementary tools.

The application of these methods could be useful when high resolution and low computational cost are required. This makes it very suitable to be implemented on microcontrollers, DSPs and logic programmable devices for future implementations in real time, for example for the development of field instruments.

References

[1] R. Arizaga, N. Cap, H.J. Rabal, M. Trivi, Display of local activity using dynamic speckle patterns, Optical Engineering 41 (2002) 287–294.
[2] I. Bloch, H. Maitre, Fuzzy mathematical morphologies: a comparative study, Pattern Recognition 28 (9) (1995) 1341–1387.
[3] E.L. Blotta, V. Ballarin, H. Rabal, Decomposition of bio-speckle signals trough granulometric size distribution, Optics Letters 34–38 (2009) 1201–1204. (ISSN: 0146-9592).
[4] E.L. Blotta, J. Pastore, V. Ballarin, H. Rabal, Classification of dynamic speckle signals through granulometric size distribution, Latin American Applied Research 39-2 (2009) 179–183. (ISSN:0327-0793).
[5] Blotta Eduardo, Ballarín Virginia, Brun Marcel, Rabal Héctor, Evaluation of speckle-interferometry descriptors to measuring drying-of-coatings, Signal Processing 91 (October (10)) (2011) 2395–2403. ISSN: 0165-1684, Elsevier North-Holland, Inc.
[6] A. Bouchet, M. Brun, V. Ballarín, Morfología matemática difusa aplicada a la segmentación de angiografías retinales, Revista Argentina de Bioingeniería 16 (Junio (1)) (2010) 7–10.
[7] R. Braga Jr., I. Dal Fabbro, F. Borem, G. Rabelo, R. Arizaga, H. Rabal, M. Trivi, Assesment of seed viability by laser speckle techniques, Biosystems Engineering 86 (3) (2003) 287–294.
[8] J.D. Briers, Sian Webster, Laser speckle contrast analysis (lasca): a nonscanning, full-field technique for monitoring capillary blood flow, Journal of Biomedical Optics 1 (2) (1996) 174–179.
[9] E.R. Dougherty, J.T. Astola, An Introduction to Nonlinear Image Processing. Tutorial Texts in Optical Engineering, SPIE Press, Bellingham, Wash, USA, 1994 TT 16.
[10] H. Dubois, D. Prade, Fuzzy Sets and Systems: Theory and Applications, Academic Press Inc, New York, 1980.
[11] A. Federico, G. Kaufmann, Evaluation of Dynamic Speckle Activity using the Empirical Mode Decomposition Method, Elsevier Science, 2006.
[12] J.G. Hampton, L. Kahre, A.J.G. Van Gastel, Quality seed from production to evaluation, Seed Science & Technology 24 (1996) 393–407.
[13] E.P. Klement, R. Mesiar, E. Pap, Triangular norms. position paper i: basic analytical and algebraic properties, Fuzzy Sets and Systems 143 (1) (2004) 5–26. Advances in Fuzzy Logic.
[14] G. Matheron, Ramdon Sets and Integral Geometry, Wiley Series in Probability and Mathematical Statistics, John Wiley & Sons, New York, NY, USA, 1975.
[15] M. Pajuelo, G. Baldwin, H. Rabal, N. Cap, R. Arizaga, M. Trivi, Bio-speckle assessment of bruising in fruits, Optics and Lasers in Engineering 40 (2003) 13–24.
[16] G.H. Sendra, R. Arizaga, H. Rabal, M. Trivi, Decomposition of biospeckle images in temporary spectral bands, Optics Letters 30 (13) (2005) 1641–1643.
[17] J. Serra, Image Analysis and Mathematical Morphology, Academic Press, 1982 vol. I.
[18] Héctor J. Rabal, Ricardo A. Arizaga, Nelly Lucía Cap, Marcelo Trivi, Graciela Romero, Elvio Alanís, Transient phenomena analysis using dynamic speckle patterns, Optical Engineering 35 (1) (1996) 57–62.